This document is confidential and is proprietary to the American Chemical Society and its authors. Do not copy or disclose without written permission. If you have received this item in error, notify the sender and delete all copies.

Modeling Multicomponent Gas Adsorption in Nanoporous Materials with Two Versions of Nonlocal Classical Density Functional Theory

Journal:	Industrial & Engineering Chemistry Research
Manuscript ID	ie-2021-029296.R1
Manuscript Type:	Article
Date Submitted by the Author:	n/a
Complete List of Authors:	Zhou, Musen; University of California Riverside Bourns College of Engineering, Chemical and Environmental Engineering Wang, Jingqi; Tsinghua University, Department of Chemical Engineering Garcia, Jose; University of California Riverside, Department of Chemical and Environmental Engineering Liu, Yu; East China University of Science and Technology, Chemical Engineering Wu, Jianzhong; University of California Riverside, Department of Chemical and Environmental Engineering

SCHOLARONE™ Manuscripts

Modeling Multicomponent Gas Adsorption in Nanoporous Materials with Two Versions of Nonlocal Classical Density Functional Theory

Musen Zhou^{1†}, Jingqi Wang^{2†}, Jose Garcia¹, Yu Liu^{3*} and Jianzhong Wu^{1*}

¹Department of Chemical and Environmental Engineering, University of California,
Riverside, CA 92521, United States, ²Department of Chemical Engineering, Tsinghua
University, Beijing, 100084, China, ³School of Chemical Engineering and Technology, Sun Yatsen University, Zhuhai, Guangdong 519000, China

Abstract

Two versions of nonlocal classical density functional theory (cDFT) have been proposed to predict multicomponent gas adsorption in nanoporous materials by using the Lennard-Jones model for gas mixtures and the universal force field for the adsorbents. With the modified fundamental measure theory to describe short-range repulsions or volume-exclusion effects, one version of cDFT adopts the mean-field approximation for van der Waals attraction (here referred to as cDFT-MFA) as commonly used in porous materials characterization, and the other version accounts for long-range correlations through a weighted-density approximation (cDFT-WDA). For a number of gas mixtures in MOF-5 (without sub-pores in accessible to gas molecules), the adsorption isotherms predicted from cDFT-WDA are quantitatively consistent with results from grand canonical Monte Carlo (GCMC) simulations, while cDFT-MFA systematically underestimates the adsorption due to neglecting the correlation effects. Nevertheless, both versions of cDFT outperform the ideal adsorbed solution theory (IAST) at high pressure. Because IAST predicts mixture adsorption using only single-component data, it fails to capture the selective behavior

[†] These authors contributed equally

^{*} To whom correspondence should be addressed. Email: jwu@engr.ucr.edu or liuyu89@mail.sysu.edu.cn

arising from asymmetric interactions among different chemical species. The cDFT calculations are implemented with massively parallel GPU-accelerated algorithms to achieve rapid yet accurate predictions of multicomponent adsorption isotherms with full atomistic details of the adsorbent materials. This work thus provides a theoretical basis for the computational design of adsorptionbased separation processes as well as for the selection and data-driven inverse design of nanoporous materials.

1. Introduction

Selective adsorption represents one of the most important industrial separation processes, with widespread applications such as desulfurization in petroleum refining, H₂ and CH₄ purification and CO₂ capture. 1-5 As chemical separation takes about half of the industrial energy use in the US, the development of more efficient processes is imperative to reduce the energy cost.⁶ Conventionally, adsorption-based separation processes are categorized into pressure swing adsorption (PSA) and temperature swing adsorption (TSA). In both cases, the adsorbent material is a dominating factor determining the separation efficiency and operation cost. Therefore, adsorbent design is of great importance in optimizing industrial separation processes.

Nanoporous materials, such as metal-organic frameworks (MOFs) and covalent-organic frameworks (COFs), are promising for adsorption separation because of their excellent mechanic stability, large surface area and adjustable pore geometry. ⁷⁻⁹ More importantly, both adsorption capacity and selectivity can be tailored for specific applications by altering the secondary building blocks of such materials. 10, 11 Compared with trial-and-error syntheses, a data-driven approach enables the inverse design of nanoporous materials over a broad range of parameters in chemical space. 12-14 However, data-driven methods require a large set of data for multicomponent adsorption isotherms. Such data are often scarce due to time-consuming experimental procedures and technical difficulties in controlling thermodynamic conditions. 15, 16

Currently thermodynamic modeling of multicomponent adsorption isotherms is mostly based on the ideal adsorbed solution theory (IAST). 17-20 Although IAST adopts ideal gas and ideal solution models for the bulk and adsorbed phases, respectively, it is able to predict the adsorption isotherms of many gas mixture systems (e.g., CH₄/C₂H₆, C₂H₄/CO₂ and CO/O₂) with the input of pure component adsorption isotherms up to moderate pressures. Many attempts have been made to modify IAST by considering surface heterogeneity and the distinct properties of gas molecules such as polarity, size and interaction energy. 21-23 Although modified IAST models are able to account for more realistic gas-absorbent interactions and improve the numerical performance, they often entail extra fitting parameters thus hamper transferability. Moreover, the modified models do not provide a consistent description of the thermodynamic non-ideality of gas mixtures in the bulk and inside the adsorbent materials, which also hinders their applications at high pressure.

Molecular simulation and statistical-mechanical methods, such as grand canonical Monte Carlo (GCMC) simulation and classical density functional theory (cDFT), are main alternatives to IAST for predicting mixture adsorption in nanoporous materials.²⁴⁻²⁷ For single-component adsorption, adsorption isotherms predicted by GCMC and cDFT are generally in good agreement with each other.²⁸⁻³¹ In contrast to the IAST models, GCMC and cDFT are able to predict adsorption isotherms for single- and multi-component systems alike. More importantly, they offer atomistic details useful for the computational design of adsorbent materials. From a practical perspective, neither GCMC nor cDFT is perfect. In addition to intrinsic errors introduced by the atomistic models, GCMC is not suitable for massive calculations due to the excessive computational burden. Conversely, cDFT is often less accurate because it relies on the formulation

of the excess Helmholtz energy functional.³²⁻³⁴ While highly reliable models for the excess Helmholtz energy functional have been developed over the past few decades to describe singlecomponent adsorption isotherms,³⁵ application of cDFT to adsorption in gas mixtures is mostly limited to slit pores³⁶⁻³⁸. Few cDFT calculations are focused on three-dimensional structures even though they are most relevant to practical applications. To bridge this gap, this work introduces two versions of cDFT for gas mixtures represented by the Lennard-Jones (LJ) model. The LJ model is often used to represent the thermodynamic properties of gas mixtures and relevant to industrial applications such as adsorption-based separation of noble gases and methane purification. ^{26, 39} Both versions of cDFT are based on the modified fundamental measure theory (MFMT) which is naturally applicable to systems containing gas molecules of different sizes. 40 With the short-range repulsions or volume-exclusion effects described by MFMT, one version of cDFT adopts the mean-field approximation (herein referred to as cDFT-MFA) to represent the excess Helmholtz energy due to van der Waals attractions, and the other accounts for the correlation effects with a weighted density approximation (herein referred to as cDFT-WDA). For single-component systems, cDFT-MFA is essentially equivalent to the nonlocal DFT (NLDFT) that is commonly used for the characterization of porous materials by gas adsorption. Both versions of cDFT are able to generate adsorption isotherms in good agreement with GCMC simulation for a wide variety of gas mixtures, while cDFT-WDA yields slightly better numerical performance because it accounts for correlation effects. Compared with IAST, both versions of cDFT predict more accurate adsorption isotherms especially at high pressure wherein gas-gas interactions and correlation effects become more significant. Because cDFT contains atomistic details for adsorbent materials and can be implemented through massively paralleled GPU programming, it empowers the rapid construction of large database potentially useful for the inverse design of nanoporous materials for gas separation.

2. Methods and Models

2.1 Classical Density Functional Theory (cDFT)

In principle, classical density functional theory (cDFT) is able to predict the thermodynamic properties of any macroscopic system at equilibrium. 41-43 In its application to multi-component gas adsorption within the Lennard-Jones (LJ) model, the grand potential is minimized with respect to the gas density profiles

$$\frac{\partial\Omega[\boldsymbol{\rho}(\mathbf{r})]}{\delta\rho_{i}(\mathbf{r})} = 0 \qquad (i = 1, 2, ..., N)$$
(1)

where N is the number of chemical species in the gas mixture, $\rho(\mathbf{r}) = [\rho_1(\mathbf{r}), \rho_2(\mathbf{r}), ..., \rho_N(\mathbf{r})]$ is a short notation for the density profiles of gas molecules, and $\mathbf{r} = (x, y, z)$ is the center-of-mass position for each gas molecule. Specifically, the grand potential can be written as

$$\Omega[\boldsymbol{\rho}(\mathbf{r})] = F[\boldsymbol{\rho}(\mathbf{r})] + \sum_{i=1}^{N} \int [V_i^{ext}(\mathbf{r}) - \mu_i^{bulk,mixture}] \rho_i(\mathbf{r}) d\mathbf{r}$$
(2)

where F is the intrinsic Helmholtz energy functional, V_i^{ext} stands for the external potential for gas component i, i.e., the potential energy on a molecule of species i due to its interaction with the absorbent, and $\mu_i^{bulk,mixture}$ represents the chemical potential for component i in the bulk phase. In this work, we use the universal force field (UFF) to describe gas interaction with nanoporous materials.⁴⁴ For the gas molecules considered in this work, the force-field parameters are provided in Support Information (SI). The modified Benedict-Webb-Rubin (MBWR) equation of state is used to calculate the chemical potentials of all species for the gas mixture in the bulk phase.⁴⁵ It should be noted that cDFT calculations are thermodynamically self-consistent even when it does

not reproduce the equation of state for the bulk fluid (e.g., MBWR). This is because the latter is only used to generate the chemical potential or bulk density as the input for the cDFT calculation. In other words, cDFT calculations can be performed without the bulk equation of state if the chemical potential is given.

The intrinsic Helmholtz energy can be divided into an ideal part and an excess:

$$F[\boldsymbol{\rho}(\mathbf{r})] = F^{id}[\boldsymbol{\rho}(\mathbf{r})] + F^{ex}[\boldsymbol{\rho}(\mathbf{r})]. \tag{3}$$

With the gas molecules represented by the LJ model, the ideal part is exactly known

$$F^{id}[\boldsymbol{\rho}(\mathbf{r})] = k_B T \sum_{i=1}^{N} \int \{\ln[\rho_i(\mathbf{r})\Lambda_i^3] - 1\} \rho_i(\mathbf{r}) d\mathbf{r}$$
(4)

where k_B stands for the Boltzmann constant, T is the absolute temperature, and Λ_i represents the thermal wavelength of component i. One essential task of all cDFT calculations is to formulate an excess Helmholtz energy functional that is reliable for the specific system under consideration. According to the LJ model, the excess Helmholtz energy can be split into contributions due to short-range repulsion and long-range attraction. The former is often represented by the hard-sphere model, F^{hs} , and a perturbation term F^{attr} is applied to account for van der Waals attractions

$$F^{ex}[\boldsymbol{\rho}(\mathbf{r})] = F^{hs}[\boldsymbol{\rho}(\mathbf{r})] + F^{attr}[\boldsymbol{\rho}(\mathbf{r})]. \tag{5}$$

As well documented, the excess Helmholtz energy of a hard-sphere system can be accurately described by the modified fundamental measure theory (MFMT)^{32, 46}

$$F^{hs}[\boldsymbol{\rho}(\mathbf{r})] = k_B T \int \Phi^{hs}[n_\alpha(\mathbf{r})] d\mathbf{r}$$
 (6)

where

$$\Phi^{hs} = -n_0 \ln(1 - n_3) + \frac{n_0 n_2 - \mathbf{n}_{V1} \cdot \mathbf{n}_{V1}}{1 - n_3} + \frac{n_3 + (1 - n_3)^2 \ln(1 - n_3)}{36\pi n_3^2 (1 - n_3)^2} \left[(n_2)^3 - 3n_2 \mathbf{n}_{V2} \cdot \mathbf{n}_{V2} \right]$$
(7)

with

$$n_{\alpha}(\mathbf{r}) = \sum_{i=1}^{N} \int \rho_{i}(\mathbf{r}') w_{i}^{(\alpha)}(|\mathbf{r} - \mathbf{r}'|) d\mathbf{r}'$$

$$\alpha \in \{0, 1, 2, 3, V1, V2\}$$
(8)

In Eq (8), $w_i^{(\alpha)}$ are a set of weight functions characterizing the differential geometry of each spherical particle:

$$\begin{cases} w_{i}^{(2)}(r) = \pi d_{i}^{2} w_{i}^{(0)}(r) \\ = 2\pi d_{i} w_{i}^{(1)}(r) \\ = \delta (d_{i} / 2 - r) \\ w_{i}^{(3)}(r) = \theta (d_{i} / 2 - r) \\ \mathbf{w}_{i}^{(V2)}(r) = 2\pi d_{i} \mathbf{w}_{i}^{(V1)}(r) = w_{i}^{(2)}(r) \frac{\mathbf{r}}{r} \end{cases}$$

$$(9)$$

where δ denotes the Dirac-delta function, θ is the Heaviside step function, and d_i is the hard-sphere diameter for component i. For all gas molecules considered in this work, the Barker-Henderson theory is used to calculate the hard-sphere diameter from the LJ parameters^{47, 48}

$$d_i = \sigma_i \left(\frac{1 + 0.2977T_i^*}{1 + 0.33163T_i^* + 0.0010477T_i^{*2}} \right)$$
 (10)

where $T_i^* = k_B T / \varepsilon_i$, ε_i and σ_i stand for the LJ energy and size parameters of the gas molecule i, respectively.

For the attraction part of the excess Helmholtz energy, one convenient choice is that from the mean-field approximation (MFA)

$$F^{MFA} = \frac{1}{2} \sum_{i=1}^{N} \sum_{j=1}^{N} \iint \rho_i(\mathbf{r}) \rho_j(\mathbf{r}') u_{ij}^{attr} (|\mathbf{r} - \mathbf{r}'|) d\mathbf{r} d\mathbf{r}'$$
(11)

where

$$u_{ij}^{attr}(r) = \begin{cases} 0 & r < \sigma_{ij} \\ 4\varepsilon_{ij} \left[\left(\frac{\sigma_{ij}}{r} \right)^{12} - \left(\frac{\sigma_{ij}}{r} \right)^{6} \right] & r > \sigma_{ij} \end{cases}$$
(12)

and the cross parameters are calculated from the Lorentz-Berthelot mixing rule. In this work, the excess Helmholtz energy given by eq (5) to (12) is referred to as cDFT-MFA. Whereas MFA is commonly used in cDFT calculations including characterization of porous materials by gas adsorption, it reduces to an equation of state for bulk systems similar to the van der Waals equation. While more accurate formulations are available for one-component LJ fluids, 49 extension of existing formulations to multicomponent systems is theoretically challenging due to the lack of analytical expressions for the bulk correlation functions.

In this work, we account for the correlation effects using van der Waals one-fluid theory (vdW1) and the weighted density approximation (WDA)^{33, 34}

$$F^{attr}[\boldsymbol{\rho}(\mathbf{r})] = F^{MFA}[\boldsymbol{\rho}(\mathbf{r})] + F^{cor}[\boldsymbol{\rho}(\mathbf{r})]$$
(13)

where F^{cor} corresponds to the local correlation Helmholtz energy

$$F^{cor}[\boldsymbol{\rho}(\mathbf{r})] = k_B T \sum_{i=1}^{N} \int \Phi^{cor}[\overline{\rho}(\mathbf{r})] d\mathbf{r}.$$
 (14)

The reduced local correlation Helmholtz energy per volume, Φ^{cor} , is approximated by that corresponding to the bulk phase at weighted density

$$\overline{\rho}(\mathbf{r}) = \sum_{i=1}^{N} \frac{3}{4\pi d_i^3} \int \rho_i(\mathbf{r'}) \theta(d_i - |\mathbf{r} - \mathbf{r'}|) d\mathbf{r'}.$$
 (15)

In the bulk phase, Φ^{cor} can be written in the following form

$$\Phi^{cor}(\rho) = \frac{F_{bulk}^{LJ}(\rho) - F_{bulk}^{hs}(\rho) - F_{bulk}^{MFA}(\rho)}{V} \beta$$
(16)

where $F_{bulk}^{LJ}(\rho)$ stands for the excess Helmholtz energy of a bulk LJ fluid calculated from the MBWR equation of state, 45 $F_{bulk}^{hs}(
ho)$ denotes the hard-sphere Helmholtz energy according to the Carnahan-Starling equation of state, 50 $F_{bulk}^{MFA}(\rho)$ represents the mean-field Helmholtz energy for the one-component fluid, and $\beta = 1/(k_B T)$. Explicit expressions are available for the hard-sphere and MF excess Helmholtz energies shown in Eq (16):

$$\beta \frac{F_{bulk}^{hs}[\overline{\rho}(\mathbf{r})]}{V} = \frac{4y - 3y^2}{(1 - y)^2} \overline{\rho}(\mathbf{r}), \tag{17}$$

$$\beta \frac{F_{bulk}^{MFA}[\bar{\rho}(\mathbf{r})]}{V} = -\frac{16}{9} \pi \beta \varepsilon_x \bar{\rho}(\mathbf{r})^2 \sigma_x^3$$
 (18)

where $y = \frac{\overline{\rho}(\mathbf{r})\pi d_x^3}{6}$. According to the vdw1 approximation, d_x , ε_x and x_i stand for the hard-sphere diameter, the LJ energy and size parameters for the mixture:

$$d_x^3 = \sum_{i=1}^N \sum_{j=1}^N \frac{\overline{\rho}_i(\mathbf{r})}{\overline{\rho}(\mathbf{r})} \frac{\overline{\rho}_j(\mathbf{r})}{\overline{\rho}(\mathbf{r})} d_{ij}^3, \tag{19}$$

$$\sigma_x^3 = \sum_{i=1}^N \sum_{j=1}^N \frac{\overline{\rho}_i(\mathbf{r})}{\overline{\rho}(\mathbf{r})} \frac{\overline{\rho}_j(\mathbf{r})}{\overline{\rho}(\mathbf{r})} \sigma_{ij}^3, \tag{20}$$

$$\varepsilon_{x} = \frac{1}{\sigma_{x}^{3}} \sum_{i=1}^{N} \sum_{j=1}^{N} \frac{\overline{\rho}_{i}(\mathbf{r})}{\overline{\rho}(\mathbf{r})} \frac{\overline{\rho}_{j}(\mathbf{r})}{\overline{\rho}(\mathbf{r})} \varepsilon_{ij} \sigma_{ij}^{3}.$$
(21)

Combing Eqs. (1) - (4) leads to the following Euler-Lagrange equations

$$\rho_{i}(\mathbf{r}) = \rho_{bulk,i} \exp\left[\beta \mu_{i}^{ex,mixture} - \beta V_{i}^{ext} - \beta \frac{\delta F^{ex}}{\delta \rho_{i}(\mathbf{r})}\right] \qquad (i = 1, 2, ..., N).$$
(22)

From Eq (22), we can calculate the density profiles of individual species for the adsorption of an N-component gas mixture in nanoporous materials. In comparison with cDFT for singlecomponent systems, the computational cost scales linearly with the number of chemical species in the gas mixture. With an explicit expression for the excess Helmholtz energy functional as given by Eqs. (5) ~ (21), we can solve the density profiles using conjugate gradient descent method.⁵¹ As explained in our previous work,⁵² the cDFT calculations can be implemented with massively paralleled algorithm through graphic processing unit (GPU). The GPU-accelerated parallel implementation drastically reduces the computational cost thereby empowering potential industrial applications. In this work, all cDFT calculations are carried out with an Nvidia Tesla P100 graphic card. The time cost is at the scale of few seconds for each cDFT calculation. More information on the computational details is given in Support Information.

2.2 Ideal Adsorbed Solution Theory (IAST)

The basic concepts and numerical procedure of ideal adsorbed solution theory (IAST) have been well documented. 17-19 Here, we recapitulate only the key equations for easy reference. With an *N*-component gas mixture inside an adsorbent represented by a two-dimensional system, pure reference states are defined for all chemical species that share the same spreading pressure of the mixture

$$\pi_1 = \pi_2 = \dots = \pi_N. \tag{23}$$

For each pure component i in equilibrium with its pure bulk phase, the spreading pressure at pressure p_i^0 can be written as:

$$\frac{\pi_i A}{RT} = \int_0^{p_i^0} \frac{n_i^0 \left(P_i\right)}{P_i} dP_i \tag{24}$$

where A is the surface area, R stands for the gas constant, T represents temperature, and n_i^0 is the adsorption amount for pure component i at its own reference state.

In analogy with the Lewis fugacity rule, IAST assumes an ideal solution for the twodimensional system of adsorbed gas molecules. The adsorbed phase would be in equilibrium with a gas mixture following the adsorption analog of Raoult's law

$$P_{i} = y_{i}P = x_{i}p_{i}^{0} \tag{25}$$

where y is the composition in the bulk phase, x represents the composition of the two-dimensional system (viz., the adsorbed gas mixture). With adsorption isotherms for single-component systems as the input, Eqs. (23) \sim (25) can be used to determine the spreading pressure and, consequently, the corresponding adsorption amount for each pure reference state as well as the compositions of the adsorbed phase. If the adsorption isotherm is fitted into a specific adsorption model (e.g. Langmuir adsorption model), Eqs. (23) \sim (25) can be solved analytically. Otherwise, it requires iteration to find p_i^0 for each chemical species such that Eqs. (23) and (25) are satisfied. An interpolation scheme would be needed to approximate the adsorption amount between the existing points on the adsorption isotherm. The total adsorption amount n_T for gas mixture is finally calculated from the ideal solution assumption

$$\frac{1}{n_T} = \sum_{i=1}^N \frac{x_i}{n_i^0} \,. \tag{26}$$

At low pressure, Henry's law predicts the adsorption selectivity

$$\frac{x_i}{x_j} = \frac{K_i}{K_j} \frac{y_i}{y_j} \tag{27}$$

where K represents Henry's constant. In this work, single-component adsorption isotherms from GCMC simulations are used as the input for the IAST prediction of multi-component adsorption isotherms. Instead of fitting the adsorption isotherm into a specific adsorption model, the direct interpolation of single-component adsorption isotherm (shown in Figure S1) is used when

calculating adsorption isotherm for mixtures in order to preserve the accuracy of adsorption isotherm at low pressure.

3. Results and Discussion

In this section, we first compare adsorption isotherms for gas mixtures and the selectivity predicted by the two versions of cDFT along with those from IAST and GCMC simulations. Computational details of GCMC simulation are provided in Supporting Information. For the calibration of the excess Helmholtz energy functions, these comparisons are discussed in the context of one particular metal-organic framework (MOF) material – MOF-5. Different from other MOFs, MOF-5 does not contain sub-pores inaccessible to small gas molecules, which may lead to an inaccurate prediction of adsorption by IAST.^{26, 53}

3.1 Adsorption at Low to Moderate Pressure

We first calibrate the cDFT predictions for binary mixtures because they provide a good benchmark for the theoretical description of mixture adsorptions. Besides, binary mixtures are important to understand the physics underlying the adsorption selectivity.

Figure 1A shows the adsorption isotherms for an equimolar mixture of Kr and Ar in MOF-5 at 297 K over a range of pressures (up to 50 bar). The symbols are from GCMC carried out in this work, and the lines are predicted from IAST and the two versions of cDFT. Because Kr and Ar molecules are similar in terms of both size and interaction energy (viz. the LJ parameters), unsurprisingly, IAST shows near quantitative performance for the adsorption amounts of both species. Previous comparisons also indicate excellent agreement between IAST and GCMC at low to moderate pressure.²⁰ The good agreement may be attributed to the similarity between different species and to the dominant effects of adsorbate-adsorbent interactions. Both the mean-field approximation (cDFT-MFA) and weighted density approximation (cDFT-WDA) predict the

adsorption isotherms in fair agreement with GCMC. While cDFT-WDA achieves a numerical performance slightly better than IAST, cDFT-MFA underestimates the adsorption amount for both Kr and Ar due to the neglect of correlation effects. In comparison with IAST, one major advantage of cDFT is that it does not require single-component adsorption isotherms as the input. Besides, it contains atomistic details that are helpful for the computational design of adsorbent materials.

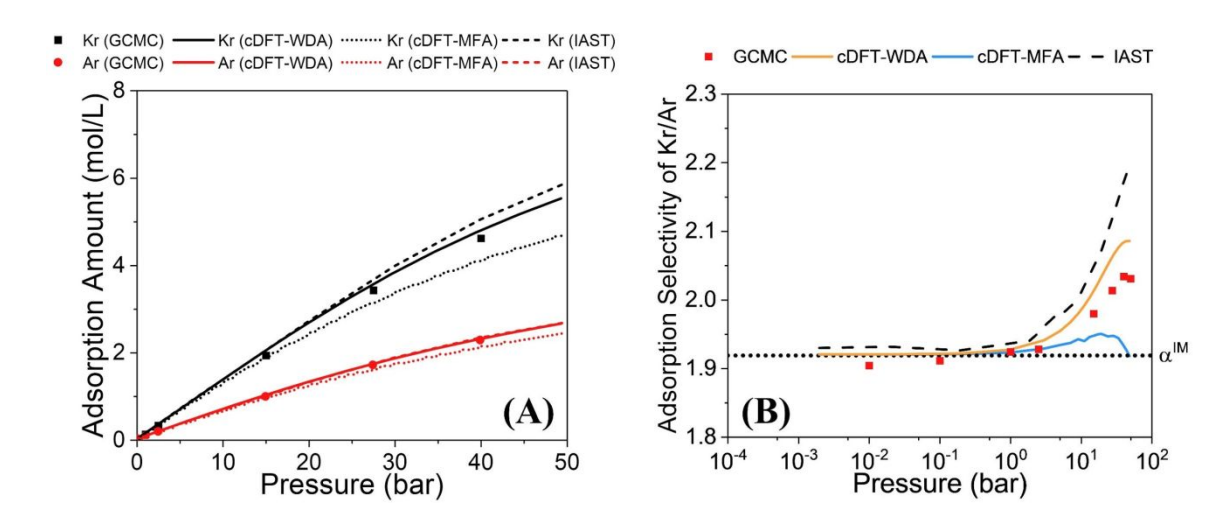


Figure 1. Adsorption amounts (A) and selectivity (B) for MOF-5 in contact with an equimolar mixture of Kr and Ar in the bulk at 297 K. In panel B, the dotted line represents the adsorption selectivity at infinite dilution.

Figure 1B shows the adsorption selectivity corresponding the adsorption isotherms shown in Figure 1A. In the limit of infinite dilution (viz, at extremely low bulk pressure), the selectivity of Kr/Ar predicted by either cDFT or by IAST converges to the ideal adsorption selectivity predicted by Henry's law. cDFT is able to reproduce the exact adsorption selectivity at infinite dilution because the excess Helmholtz energy vanishes in the ideal limit. In principle, IAST is also able to reproduce the ideal limit if highly accurate data are available for pure-component adsorption isotherms at infinite dilution.²⁶ However, the procedure is numerically problematic and requires much more iterations in GCMC simulations because small adsorption amount at low pressure leads

to large errors in the adsorption selectivity. With the increase of pressure, cDFT-WDA predicts the adsorption selectivity still in quantitative agreement with that from GCMC simulation while IAST shows noticeable deviations. In contrast, cDFT-MFA underestimates the adsorption amount for Kr and predicts unreasonable adsorption selectivity at moderate pressure. For other binary mixtures with more distinct physiochemical properties (e.g., CH₄/CO₂), we observe similar trends in adsorption isotherm and selectivity at low to moderate pressures (shown in Figure S2).

Practical applications of adsorption-based separation processes are often concerned with gas mixtures beyond binary systems (e.g., H₂/N₂/CO/CH₄/CO₂ in hydrogen purification). The adsorbate-adsorbate interactions become more complicated when there are more components in the mixture.³⁹ Therefore, in addition to binary gas mixtures, we also calibrate the cDFT methods with a ternary system, H₂/CH₄/CO₂, which has distinct size and interaction energy differences among different species. Figure 2 shows the adsorption isotherms at 313.15 K. Similar to that observed for the binary gas mixture, both IAST and cDFT-WDA slightly overestimate the simulation data for the highly adsorbed component (viz., CO₂) while giving excellent predictions of the adsorption amount for the other two components (H₂/CH₄). However, cDFT-MFA underestimates the adsorption amount for both CO₂ and CH₄. In terms of the adsorption selectivity, IAST and both versions of cDFT are able to reproduce the results from GCMC simulation. It is also worth mentioning that, compared with experimental measurement in literature^{15, 54}, the adsorption behavior (viz. adsorption amount) of gas mixture in MOF-5 is well captured by the force field parameters adapted in this work (shown in Figure S3), which indicates its direct relevance to the practical applications.

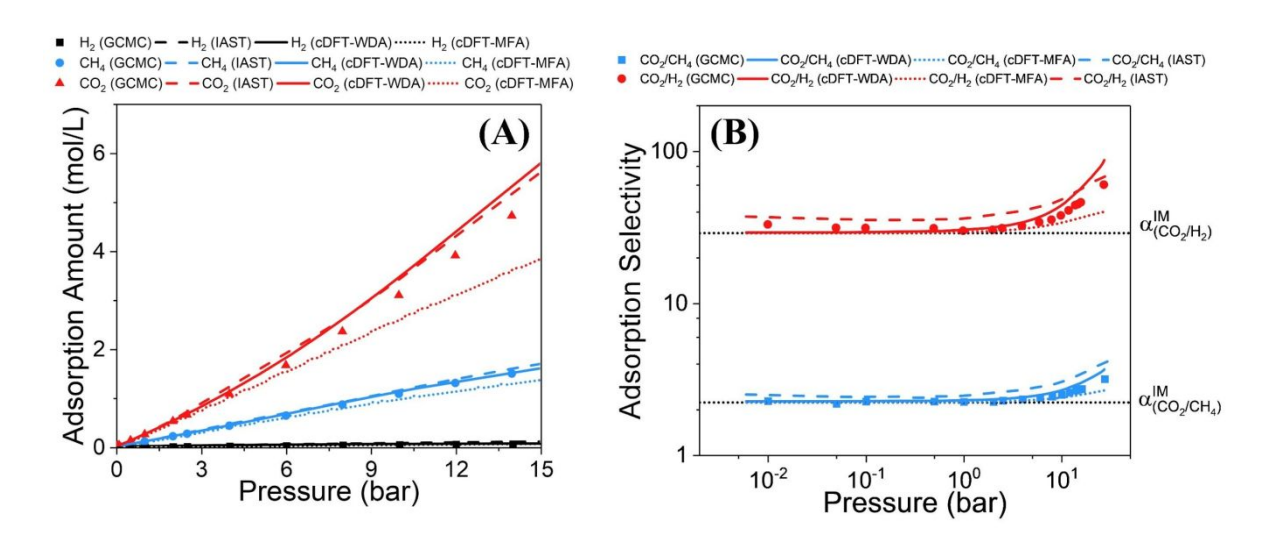


Figure 2. Adsorption isotherms (A) and selectivity (B) for a ternary mixture of H₂, CH₄ and CO₂ in MOF-5 at 313.15 K with the molar ratios in the bulk given by H₂:CH₄:CO₂=15:42.5:42.5. In panel B, the dotted line represents the adsorption selectivity at infinite dilution.

3.2 Adsorption at High Pressure

Industrial applications of adsorption-based separation are mostly operated between low and moderate pressures (under 100 bar). Under those conditions, the IAST performance has been proven to be reasonable. ^{17, 20} However, separation of gas mixtures from power plants, especially when the process is built on the integrated gasification combined cycle (IGCC), is often carried out under higher pressure (up to 200 bar). ¹⁶ Owing to their excellent mechanic stability and thermal stability, many MOFs are promising to serve as effective adsorbents for those processes. To facilitate selection and computational design of MOFs, computational methods are needed for fast and accurate evaluation of adsorption isotherms and selectivity at high pressures.

Figure 3 shows the adsorption isotherms and selectivity for an equimolar gas mixture of Kr and Ar in MOF-5 at 297 K up to 450 bar of the bulk pressure. Although IAST shows good performance for the bulk pressure up to 50 bar, with the further increase of the bulk pressure, it over- and under-estimates the adsorption amounts of Kr and Ar, respectively. It is somewhat

surprising that IAST fails to predict the adsorption isotherm at high pressure even for gas mixtures of similar molecular size and interaction energy. At high pressures, not only does the assumption of ideal solution break down, but the two-dimensional model is also problematic due to the significant inhomogeneity of gas densities inside the pores. Compared with the adsorption isotherms calculated from GCMC simulation, both versions of cDFT perform better than IAST at high pressure. While the cDFT predictions of the adsorption amount are near perfect for Ar, noticeable differences are seen between cDFT-WDA and cDFT-MFA predictions for Kr, which slightly over- and under-estimates the adsorption amount, respectively, in comparison with the simulation data. Figure 3B shows that cDFT-WDA yields a much better selectivity than cDFT-MFA while IAST yields only semi-quantitative predictions.

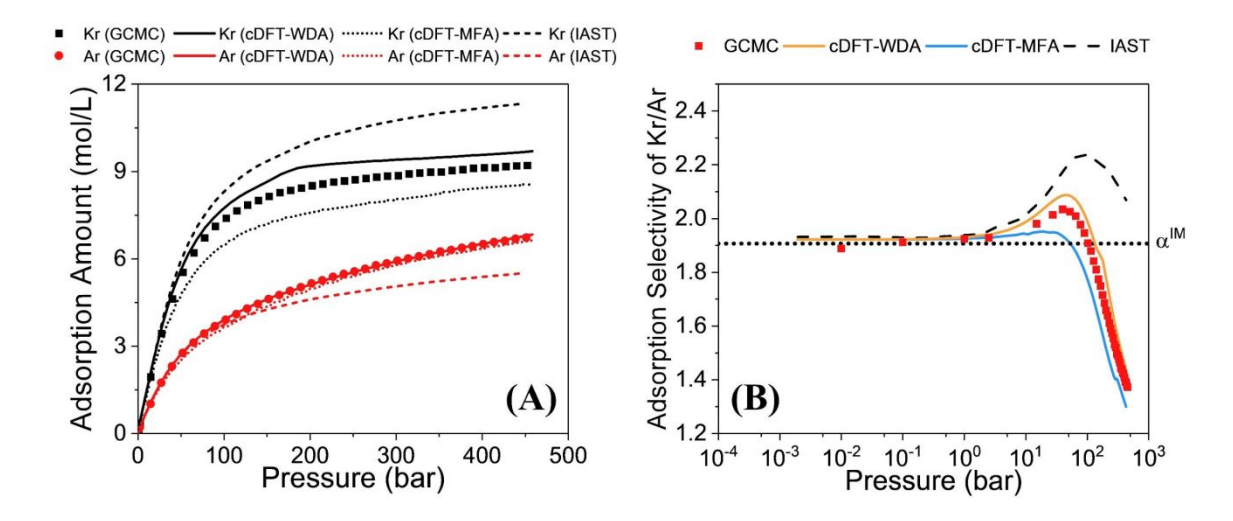


Figure 3. Adsorption isotherms (A) and selectivity (B) for an equimolar mixture of Kr and Ar in MOF-5 at 297 K. In Panel B, the dotted line represents the adsorption selectivity at infinite dilution.

For gas mixtures containing molecules with asymmetry in both size and interaction energy, the difference of adsorbate-adsorbate interactions is magnified at high pressure. As a result, the ideal-solution assumption becomes more problematic as the number of components increases. Figure 4 compares the adsorption isotherms and selectivity calculated from GCMC with those predicted by

cDFT and IAST for a ternary mixture of H₂, CH₄ and CO₂ (with molar ratios in the bulk H₂:CH₄:CO₂=15:42.5:42.5) in MOF-5 at 313.15 K. While cDFT-WDA is able to predict both the adsorption amounts and selectivity in quantitative agreement with the simulation results for the entire range of pressure, the predictions by cDFT-MFA are mostly semi-quantitative. Similar to the adsorption of an equimolar binary gas mixture of CH₄ and CO₂ (shown in Figure S4), the increase of pressure reduces the adsorption amount for CO₂ beyond a certain value while the adsorptions of CH₄ and H₂ keep on increasing as pressure rises. As CH₄ and H₂ molecules are smaller compared with CO₂, the favorable adsorption sites (near the corners of the MOF pores) are more likely to be further occupied by CH₄ or H₂ than CO₂ at high gas pressure (shown in Figure S5).⁵⁵ The maximum CO₂ adsorption amount at 115 bar is captured by both versions of cDFT but not by IAST. More specifically, cDFT-WDA quantitatively captures the competitive adsorption behavior while cDFT-MFA underestimates the adsorption amount for both CO₂ and H₂.

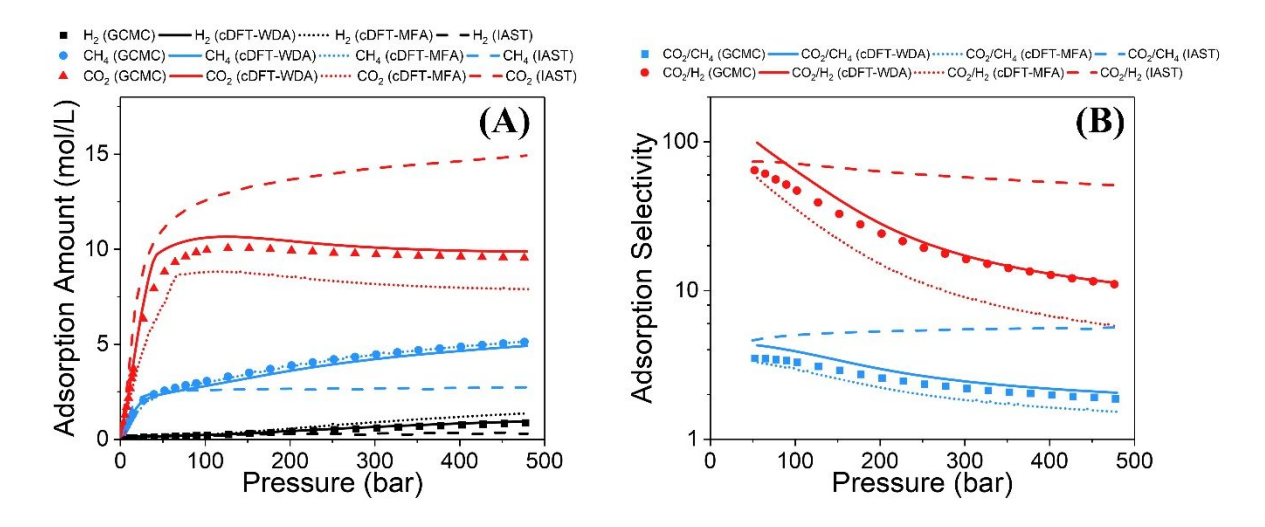


Figure 4. Adsorption isotherms (A) and selectivity (B) for a ternary mixture of H₂, CH₄ and CO₂ in MOF-5 at 313.15 K with bulk molar ratios of H₂:CH₄:CO₂=15:42.5:42.5. In Panel B, the dotted line represents the adsorption selectivity at infinite dilution.

For the ternary mixture considered in this work, CO₂ and CH₄ have the same composition in the bulk phase. Interestingly, the presence of H₂ has different effects on the adsorptions of CH₄ and CO₂. Compared with the equimolar binary gas mixture CH₄/CO₂ (shown in Figure S4), H₂ has a stronger effect on CH₄ adsorption than that on CO₂ because these gas molecules have different favorable adsorption sites. The favorable adsorption site for H₂ is closer to that of CH₄ than that of CO₂ (shown in Figure S5). As a result, the competition between CH₄ and H₂ adsorptions is more significant than that between CO₂ and H₂.

Compared with the results from GCMC simulation, both cDFT-WDA and cDFT-MFA make near quantitative predictions of the selectivity at high pressure. As that for the binary systems, cDFT-WDA gives a better prediction than cDFT-MFA. In the bulk limit, cDFT-WDA reduces to the MBWR equation, which is a well-tested equation of state, while cDFT-MFA yields only qualitative results as one may expect from the van der Waals equation. In contrast to cDFT predictions, the results from IAST are not even qualitative for the selectivity of CO₂/CH₄ at high pressure due to the neglect of adsorbate-adsorbate interactions.

3.3 Adsorption sites and density isosurfaces

As mentioned above, cDFT gives not only adsorption isotherms and selectivity but also full atomistic details useful for adsorbent design. The adsorption sites for different adsorbates can be identified from the density isosurfaces. For example, Figure 5 shows the density profiles of CH₄, CO₂ and H₂ predicted by cDFT-WDA for the ternary gas mixture with molar composition (H₂:CH₄:CO₂=15:42.5:42.5) in MOF-5 at 313.15 K and the bulk pressure of 100 bar and 300 bar. At 100 bar, the gas molecules are mainly localized on the favorable adsorption sites. The local density of CO₂ is much higher than those of H₂ and CH₄, which explains the stronger adsorption of CO₂ than that of H₂ or CH₄. When the bulk pressure increases to 300 bar, the densities of CH₄ and H₂ extend to the pore centers and that of CO₂ declines, indicating that the favorable adsorption sites for CO₂ are more likely to be occupied by smaller gas molecules (i.e., CH₄ and H₂). In other words, the favorable adsorption sites taken by H₂ and CH₄ molecules repel CO₂ molecules, resulting in the reduction of the CO₂ adsorption in the isotherm.

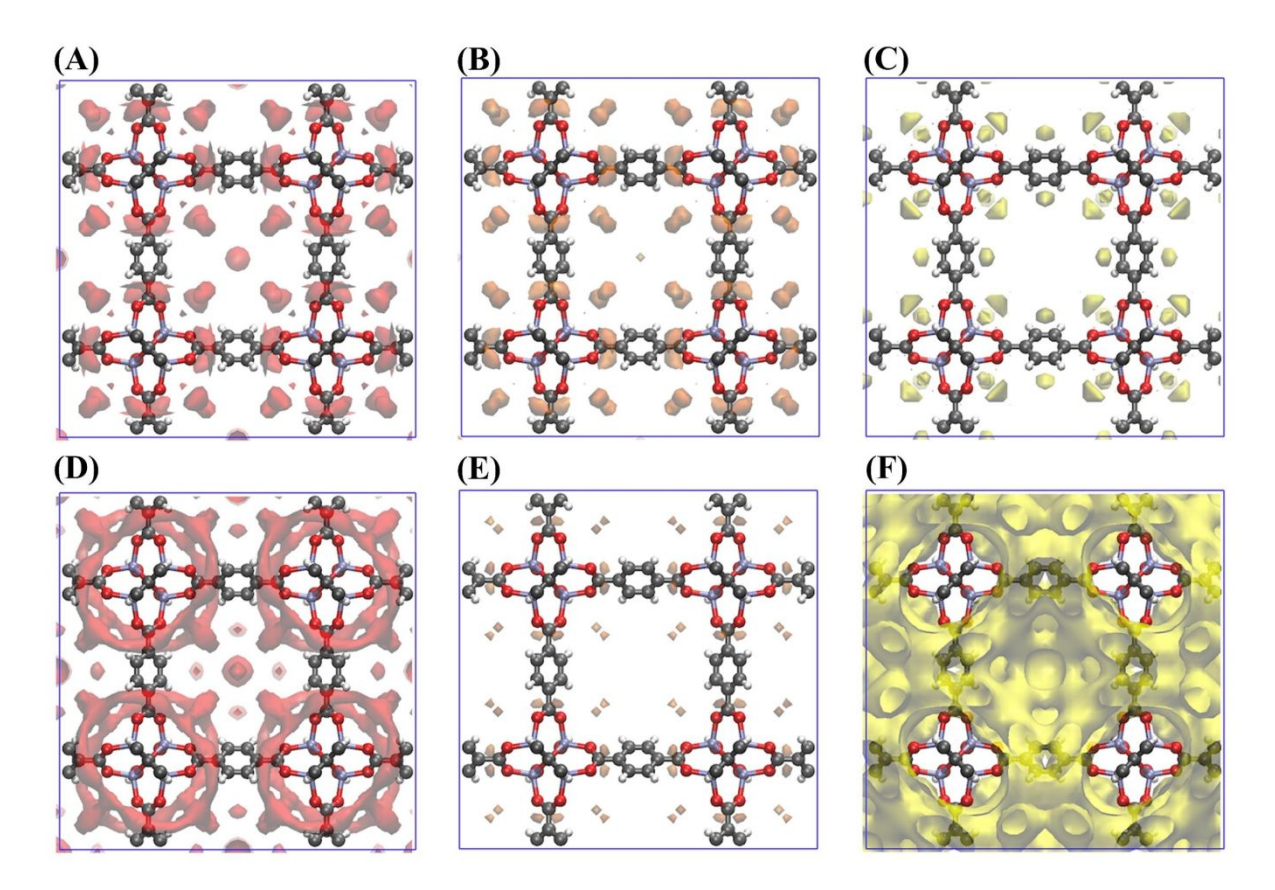


Figure 5. Density isosurfaces of CH₄, CO₂ and H₂ in MOF-5 for the adsorption of a ternary mixture with bulk molar composition (H₂:CH₄:CO₂=15:42.5:42.5) predicted by cDFT-WDA at 313.15 K and the gas pressure of 100 bar (top) and 300 bar (bottom). The red isosurfaces in (A) and (D) are for CH₄ with the local density of 0.017 molecules/Å³. The orange isosurfaces in (B) and (E) are for CO₂ with the local density of 0.09 molecules/Å³. The yellow isosurfaces in (C) and (F) are for H₂ with the local density of 0.0005 molecules/Å³. The grey, purple, red and white spheres represent carbon, zinc, oxygen and hydrogen atoms, respectively.

With atomistic information for mixture adsorption available from cDFT, we can identify favorable adsorption sites in the complex structure not only for existing nanoporous materials, but also for in-silico designed nanoporous materials before synthesis. Clearly, the density isosurface is beyond the simple geometry analysis (e.g., pore size distribution) yet offers direct insights when designing new nanoporous materials for specific applications. For example, to remove even more CO₂ from ternary mixture of H₂, CH₄ and CO₂ at high pressure, one may substitute the metal node and organic linker in MOF-5 with smaller secondary building blocks that allow for more adsorption of CO₂ according to favorable adsorption sites identified from Figure 5.

Finally, it is worth emphasizing that the main advantage of cDFT over GCMC is the computational efficiency. For example, Figure 6 shows the computation time of GCMC, cDFT-MFA and cDFT-WDA for equimolar binary mixture of Kr and Ar. Also shown in Figure 6 are the speedup factors of cDFT-MFA and cDFT-WDA compared with GCMC simulation. The computational time and speedup factor for ternary mixture of H₂, CH₄ and CO₂ are shown in Figure S6. As discussed in an earlier work⁵², all cDFT calculations were executed with massively paralleled GPU-accelerated implementation on Nvidia Tesla P100 graphic card with one CPU core on Intel Xeon E5-2620 v4. Meanwhile, all GCMC simulations are carried via RASPA with one CPU core on Intel Xeon E5-2640 v4. With massively paralleled GPU-accelerated implementation, both cDFT-MFA and cDFT-WDA are 2~3 orders of magnitude faster than serial GCMC simulation for typical binary and ternary mixtures at moderate pressure, and the speedup becomes even more noticeable at higher pressure. The detailed discussion of this implementation can be found in our previous work.⁵² Even compared with parallel GCMC code with GPU acceleration such as GPU Optimized Monte Carlo (GOMC)⁵⁶, massively paralleled GPU-accelerated cDFT is still much faster. For GOMC, the speedup factor is up to 30 while massively paralleled GPU-

accelerated cDFT can achieve speedup factor up to several hundreds⁵². Compared with cDFT-MFA, cDFT-WDA takes correlation effect into account and the extra correlation term needs to be re-evaluated in each iteration, which results in a slight increase of the computation time. Although the computational cost of cDFT increases proportional to the number of components, all the calculations can be finished within few seconds even for ternary mixtures. The rapid and accurate evaluation of multicomponent adsorption isotherms is essential for the construction of large database for data-driven materials design.

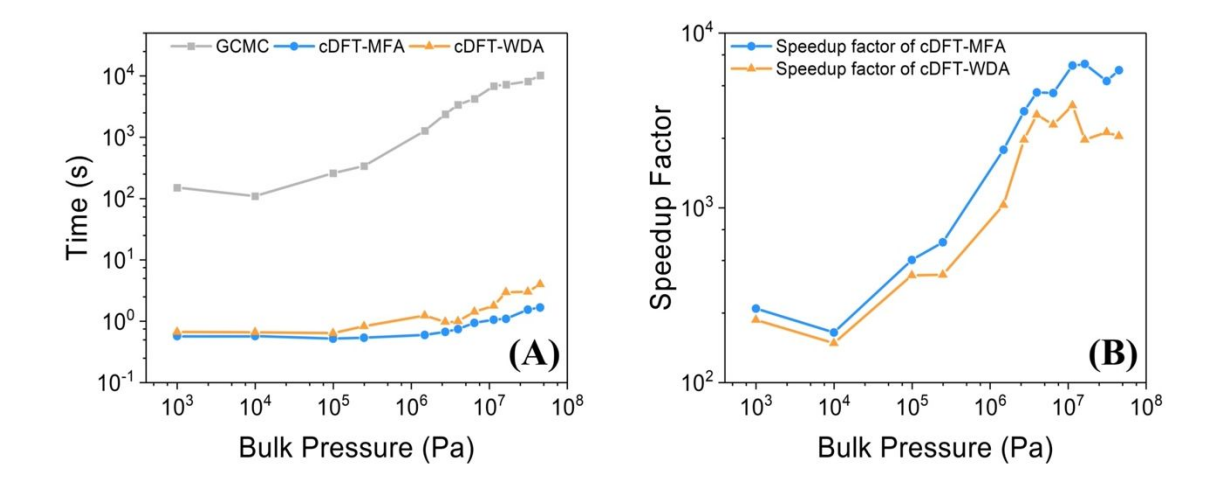


Figure 6. (A) Computation time of GCMC, cDFT-MFA and cDFT-WDA versus system pressure for equimolar binary mixture of Kr and Ar. (B) The speedup factors of cDFT-MFA and cDFT-WDA are based on the computation time of GCMC.

4. Conclusion

In this work, we propose two versions of classical density functional theory (cDFT) for describing adsorption of multicomponent gas mixtures by nanoporous materials. Their main difference lies in the formulation of the excess Helmholtz energy due to van der Waals attraction. One is based on the mean-field approximation (cDFT-MFA), which is commonly used in cDFT calculations and has been adopted in porous materials characterization. The other accounts for the correlation effects by using the weighted density approximation (cDFT-WDA). The two

formulations of the excess Helmholtz energy have been tested for both binary and ternary systems. Compared with the results from grand canonical Monte Carlo (GCMC) simulations, cDFT-WDA is able to predict both the adsorption isotherms and selectivity near quantitatively. However, cDFT-MFA significantly underestimates the adsorption amount due to the absence of the correlation contribution to the excess Helmholtz energy. Compared with the ideal adsorbed solution theory (IAST), both versions of cDFT show substantial improvements, especially at high pressure where adsorbate-adsorbate interactions and correlation effects become more significant. At low pressure, both two versions of cDFT and IAST can quantitatively predict the adsorption isotherm and selectivity. Moreover, cDFT offers atomistic details revealing the underlying mechanism of competitive adsorption in gas mixtures, which well explains the peak adsorption in CO₂. The microscopic insights are instrumental to the computational design of nanoporous materials for more efficient separation of multicomponent gas mixtures by adsorption. In addition, with the massively parallel GPU-accelerated implementation, both cDFT calculations can be accomplished at the scale of few seconds for each thermodynamic condition, which is a few orders of magnitude faster than GCMC simulation. Therefore, cDFT may be used as an alternative to IAST or GCMC for constructing a large and accurate adsorption database for multicomponent gas mixtures that are needed for the data-driven inverse design of nanoporous materials.

Supporting Information

It provides the computational details of grand canonical Monte Carlo (GCMC) simulation and classical density functional theory for predicting the adsorption of multicomponent gas mixtures in nanoporous materials, including the adsorption isotherms and selectivity for CO₂/CH₄, additional density isosurfaces for CH₄/CO₂/H₂ in MOF-5 at 313.15 K and 100 bar and computational expense comparison for ternary mixture.

Acknowledgement

This work is financially supported by the National Science Foundation's Harnessing the Data Revolution (HDR) Big Ideas Program under Grant No. NSF 1940118. Y.L acknowledges supports from the National Natural Science Foundation of China (No. 21776070).

Notes

The input data and computer codes for generating the results reported in this article are available from Zenodo (10.5281/zenodo.5528311).

Reference

- 1. Aaron, D.; Tsouris, C., Separation of CO2 from flue gas: A review. *Sep Sci Technol* **2005**, 40, (1-3), 321-348.
- 2. Ritter, J. A.; Ebner, A. D., State-of-the-art adsorption and membrane separation processes for hydrogen production in the chemical and petrochemical industries. *Sep Sci Technol* **2007**, 42, (6), 1123-1193.
- 3. Sircar, S.; Golden, T. C., Purification of hydrogen by pressure swing adsorption. *Sep Sci Technol* **2000**, 35, (5), 667-687.
- 4. Saha, D.; Grappe, H. A.; Chakraborty, A.; Orkoulas, G., Postextraction Separation, On-Board Storage, and Catalytic Conversion of Methane in Natural Gas: A Review. *Chem Rev* **2016**, 116, (19), 11436-11499.
- 5. Barelli, L.; Bidini, G.; Gallorini, F.; Servili, S., Hydrogen production through sorption-enhanced steam methane reforming and membrane technology: A review. *Energy* **2008**, 33, (4), 554-570.
- 6. Sholl, D. S.; Lively, R. P., Seven chemical separations to change the world. *Nature* **2016**, 532, (7600), 435-7.

- 7. Li, J. R.; Kuppler, R. J.; Zhou, H. C., Selective gas adsorption and separation in metalorganic frameworks. *Chem Soc Rev* **2009**, 38, (5), 1477-504.
- 8. Feng, X.; Ding, X.; Jiang, D., Covalent organic frameworks. *Chem Soc Rev* **2012**, 41, (18), 6010-6022.
- 9. Ozekmekci, M.; Salkic, G.; Fellah, M. F., Use of zeolites for the removal of H2S: A minireview. *Fuel Process Technol* **2015**, 139, 49-60.
- 10. Chong, S.; Lee, S.; Kim, B.; Kim, J., Applications of machine learning in metal-organic frameworks. *Coordin Chem Rev* **2020**, 423, 213487.
- 11. Yao, Z. P.; Sanchez-Lengeling, B.; Bobbitt, N. S.; Bucior, B. J.; Kumar, S. G. H.; Collins, S. P.; Burns, T.; Woo, T. K.; Farha, O. K.; Snurr, R. Q.; Aspuru-Guzik, A., Inverse design of nanoporous crystalline reticular materials with deep generative models. *Nat Mach Intell* **2021**, 3, (1), 76-86.
- 12. Chung, Y. G.; Gomez-Gualdron, D. A.; Li, P.; Leperi, K. T.; Deria, P.; Zhang, H.; Vermeulen, N. A.; Stoddart, J. F.; You, F.; Hupp, J. T.; Farha, O. K.; Snurr, R. Q., In silico discovery of metal-organic frameworks for precombustion CO2 capture using a genetic algorithm. *Sci Adv* **2016**, 2, (10), e1600909.
- 13. Simon, C. M.; Mercado, R.; Schnell, S. K.; Smit, B.; Haranczyk, M., What are the best materials to separate a xenon/krypton mixture? *Chem Mater* **2015**, 27, (12), 4459-4475.
- 14. Simon, C. M.; Kim, J.; Gomez-Gualdron, D. A.; Camp, J. S.; Chung, Y. G.; Martin, R. L.; Mercado, R.; Deem, M. W.; Gunter, D.; Haranczyk, M.; Sholl, D. S.; Snurr, R. Q.; Smit, B., The materials genome in action: identifying the performance limits for methane storage. *Energy Environ Sci* **2015**, 8, (4), 1190-1199.

- 15. Kloutse, F.; Hourri, A.; Natarajan, S.; Benard, P.; Chahine, R., Experimental benchmark data of CH4, CO2 and N2 binary and ternary mixtures adsorption on MOF-5. *Sep Purif Technol* **2018,** 197, 228-236.
- 16. Ullah, R.; Saad, M. A. H. S.; Aparicio, S.; Atilhan, M., Adsorption equilibrium studies of CO2, CH4 and N2 on various modified zeolites at high pressures up to 200 bars. *Microporous Mesoporous Mater* **2018**, 262, 49-58.
- 17. Walton, K. S.; Sholl, D. S., Predicting multicomponent adsorption: 50 years of the ideal adsorbed solution theory. *AIChE J* **2015**, 61, (9), 2757-2762.
- 18. Myers, A. L.; Prausnitz, J. M., Thermodynamics of mixed-gas adsorption. *AIChE J* **1965**, 11, (1), 121-127.
- 19. Simon, C. M.; Smit, B.; Haranczyk, M., pyIAST: Ideal adsorbed solution theory (IAST) Python package. *Comput Phys Commun* **2016**, 200, 364-380.
- 20. Cessford, N. F.; Seaton, N. A.; Duren, T., Evaluation of Ideal Adsorbed Solution Theory as a Tool for the Design of Metal-Organic Framework Materials. *Ind Eng Chem Res* **2012**, 51, (13), 4911-4921.
- 21. Wang, K.; Qiao, S. Z.; Hu, X. J., On the performance of HIAST and IAST in the prediction of multicomponent adsorption equilibria. *Sep Purif Technol* **2000**, 20, (2-3), 243-249.
- 22. Sakuth, M.; Meyer, J.; Gmehling, J., Measurement and prediction of binary adsorption equilibria of vapors on dealuminated Y-zeolites (DAY). *Chem Eng Process* **1998**, 37, (4), 267-277.
- 23. Costa, E.; Sotelo, J.; Calleja, G.; Marron, C., Adsorption of binary and ternary hydrocarbon gas mixtures on activated carbon: experimental determination and theoretical prediction of the ternary equilibrium data. *AIChE J* **1981,** 27, (1), 5-12.

- 24. Ryan, P.; Farha, O. K.; Broadbelt, L. J.; Snurr, R. Q., Computational Screening of Metal-Organic Frameworks for Xenon/Krypton Separation. *AIChE J* **2011**, 57, (7), 1759-1766.
- 25. Gurdal, Y.; Keskin, S., A new approach for predicting gas separation performances of MOF membranes. *J Membr Sci* **2016**, 519, 45-54.
- 26. Van Heest, T.; Teich-McGoldrick, S. L.; Greathouse, J. A.; Allendorf, M. D.; Sholl, D. S., Identification of Metal–Organic Framework Materials for Adsorption Separation of Rare Gases: Applicability of Ideal Adsorbed Solution Theory (IAST) and Effects of Inaccessible Framework Regions. *J Phys Chem C* **2012**, 116, (24), 13183-13195.
- 27. Fu, J.; Tian, Y.; Wu, J. Z., Classical density functional theory for methane adsorption in metal-organic framework materials. *AIChE J* **2015**, 61, (9), 3012-3021.
- 28. Bristow, J. K.; Tiana, D.; Walsh, A., Transferable Force Field for Metal-Organic Frameworks from First-Principles: BTW-FF. *J Chem Theory Comput* **2014**, 10, (10), 4644-4652.
- 29. Bureekaew, S.; Amirjalayer, S.; Tafipolsky, M.; Spickermann, C.; Roy, T. K.; Schmid, R., MOF-FF A flexible first-principles derived force field for metal-organic frameworks. *Phys Status Solidi B* **2013**, 250, (6), 1128-1141.
- 30. Witman, M.; Wright, B.; Smit, B., Simulating Enhanced Methane Deliverable Capacity of Guest Responsive Pores in Intrinsically Flexible MOFs. *J Phys Chem Lett* **2019**, 10, (19), 5929-5934.
- 31. Bousquet, D.; Coudert, F. X.; Boutin, A., Free energy landscapes for the thermodynamic understanding of adsorption-induced deformations and structural transitions in porous materials. *J Chem Phys* **2012**, 137, (4), 044118.
- 32. Yu, Y. X.; Wu, J. Z., Structures of hard-sphere fluids from a modified fundamental-measure theory. *J Chem Phys* **2002**, 117, (22), 10156-10164.

- 33. Yu, Y. X., A novel weighted density functional theory for adsorption, fluid-solid interfacial tension, and disjoining properties of simple liquid films on planar solid surfaces. *J Chem Phys* **2009**, 131, (2), 024704.
- 34. Liu, Y.; Liu, H.; Hu, Y.; Jiang, J., Development of a density functional theory in three-dimensional nanoconfined space: H2 storage in metal-organic frameworks. *J Phys Chem B* **2009**, 113, (36), 12326-31.
- 35. Wu, J., Density functional theory for liquid structure and thermodynamics. In *Molecular thermodynamics of complex systems*, Lu, X.; Hu, Y.; Chen, H., Eds. Springer: Berlin, 2009; pp 1-74.
- 36. Motevaselian, M.; Aluru, N., An EQT-based cDFT approach for thermodynamic properties of confined fluid mixtures. *J Chem Phys* **2017**, 146, (15), 154102.
- 37. Camacho Vergara, E. L.; Kontogeorgis, G. M.; Liang, X., Gas adsorption and interfacial tension with classical density functional theory. *Ind Eng Chem Res* **2019**, 58, (14), 5650-5664.
- 38. Sauer, E.; Gross, J., Classical Density Functional Theory for Liquid-Fluid Interfaces and Confined Systems: A Functional for the Perturbed-Chain Polar Statistical Associating Fluid Theory Equation of State. *Industrial & Engineering Chemistry Research* **2017**, 56, (14), 4119-4135.
- 39. Krishna, R., Metrics for Evaluation and Screening of Metal-Organic Frameworks for Applications in Mixture Separations. *ACS Omega* **2020**, 5, (28), 16987-17004.
- 40. Yu, Y. X.; Wu, J. Z., A modified fundamental measure theory for spherical particles in microchannels. *J Chem Phys* **2003**, 119, (4), 2288-2295.
 - 41. Wu, J., Variational Methods in Molecular Modeling. Springer: 2016.

- 42. Wu, J.; Li, Z., Density-functional theory for complex fluids. *Annu Rev Phys Chem* **2007**, 58, 85-112.
- 43. Wu, J., Density functional theory for chemical engineering: From capillarity to soft materials. *AIChE J* **2006**, 52, (3), 1169-1193.
- 44. Rappe, A. K.; Casewit, C. J.; Colwell, K. S.; Goddard, W. A.; Skiff, W. M., Uff, a Full Periodic-Table Force-Field for Molecular Mechanics and Molecular-Dynamics Simulations. *J Am Chem Soc* **1992**, 114, (25), 10024-10035.
- 45. Johnson, J. K.; Zollweg, J. A.; Gubbins, K. E., The Lennard-Jones Equation of State Revisited. *Mol Phys* **1993**, 78, (3), 591-618.
- 46. Roth, R.; Evans, R.; Lang, A.; Kahl, G., Fundamental measure theory for hard-sphere mixtures revisited: the White Bear version. *J Phys: Condens Matter* **2002**, 14, (46), 12063.
- 47. Henderson, D., Monte Carlo and perturbation theory studies of the equation of state of the two-dimensional Lennard-Jones fluid. *Mol Phys* **1977**, 34, (2), 301-315.
- 48. Cotterman, R. L.; Schwarz, B. J.; Prausnitz, J. M., Molecular thermodynamics for fluids at low and high densities. Part I: Pure fluids containing small or large molecules. *AIChE J* **1986,** 32, (11), 1787-1798.
- 49. Fu, J.; Liu, Y.; Tian, Y.; Wu, J. Z., Density Functional Methods for Fast Screening of Metal Organic Frameworks for Hydrogen Storage. *J Phys Chem C* **2015**, 119, (10), 5374-5385.
- 50. Carnahan, N. F.; Starling, K. E., Equation of state for nonattracting rigid spheres. *J Chem Phys* **1969**, 51, (2), 635-636.
- 51. Hager, W. W.; Zhang, H. C., Algorithm 851: CG DESCENT, a conjugate gradient method with guaranteed descent. *Acm T Math Software* **2006,** 32, (1), 113-137.

- 52. Zhou, M.; Wu, J., A GPU implementation of classical density functional theory for rapid prediction of gas adsorption in nanoporous materials. *J Chem Phys* **2020**, 153, (7), 074101.
- 53. Babarao, R.; Dai, S.; Jiang, D. E., Effect of Pore Topology and Accessibility on Gas Adsorption Capacity in Zeolitic-Imidazolate Frameworks: Bringing Molecular Simulation Close to Experiment. *J Phys Chem C* **2011**, 115, (16), 8126-8135.
- 54. Kloutse, F.; Hourri, A.; Natarajan, S.; Benard, P.; Chahine, R., Hydrogen separation by adsorption: Experiments and modelling of H2-N2-CO2 and H2-CH4-CO2 mixtures adsorption on CuBTC and MOF-5. *Microporous Mesoporous Mater* **2018**, 271, 175-185.
- 55. Zhou, W.; Zhang, Z.; Wang, H.; Yan, Y.; Liu, X., Molecular insights into competitive adsorption of CO 2/CH 4 mixture in shale nanopores. *RSC Adv* **2018**, 8, (59), 33939-33946.
- 56. Nejahi, Y.; Barhaghi, M. S.; Mick, J.; Jackman, B.; Rushaidat, K.; Li, Y.; Schwiebert, L.; Potoff, J., GOMC: GPU Optimized Monte Carlo for the simulation of phase equilibria and physical properties of complex fluids. *SoftwareX* **2019**, *9*, 20-27.

TOC Graphic

